Results in Chemistry 28 (2026) 103615

Contents lists available at ScienceDirect

Results in Chemistry

journal homepage: www.sciencedirect.com/journal/results-in-chemistry

Room-temperature chitosan-assisted *in situ* formation of silver nanoparticles on citric-acid-functionalized cotton for wash-durable antibacterial activity

A. D'Agostino [a,*], S. Facchiano [b], C. Vineis [b], M. Hadhri [a], R. Palucci Rosa [a], G. Rosace [a,c], A. Safarshargh [a], V. Trovato [a,c]

[a] Department of Engineering and Applied Sciences, University of Bergamo, Dalmine, Italy
[b] Institute of Intelligent Industrial Technologies and Systems for Advanced Manufacturing - National Research Council (STIIMA-CNR), CNR, Biella, Italy
[c] Local CSGI (Inter-University Center for Colloid and Surface Science) Research Unit, Dalmine, Italy

ARTICLE INFO

Keywords:
Silver nanoparticles
Chitosan
Cotton
In situ green synthesis
Antibacterial finishing

ABSTRACT

Antibacterial textiles are increasingly investigated to mitigate microbial proliferation and improve hygiene, particularly in healthcare and protective applications. Here, a simple water-based, partly bio-based three-step strategy is presented to fabricate laundering-durable antibacterial cotton *via* citric-acid pre-functionalization and chitosan-assisted *in situ* formation of silver nanoparticles (AgNPs). Cotton fabrics were first grafted with citric acid to introduce carboxyl-binding sites, then loaded with Ag^{+} from $AgNO_3$, and finally treated with chitosan, which served as a bio-based reducing and stabilizing agent enabling the formation of AgNPs at room temperature. CIE L*a*b* colorimetric analysis revealed formulation-dependent variations in lightness and chromaticity consistent with optical effects associated with AgNPs. SEM-EDX confirmed a homogeneous distribution of Ag-rich surface domains on the fibre surface, while FTIR and Raman spectroscopy indicated preservation of the main cellulose fingerprints, suggesting limited alteration of fibre chemistry. The functionalized fabrics exhibited >99% antibacterial activity against *Staphylococcus aureus* and *Escherichia coli* in the unwashed state, with selected formulations retaining >95% efficacy after 10 standardized laundering cycles. Overall, this bio-based approach, enabling AgNPs formation at room temperature, offers a practical route to durable antibacterial cotton with high wash fastness, making it a promising candidate for a wide range of applications across fields such as health and medicine.

1. Introduction

Textiles are among the most widely used materials in both industrial and domestic applications. In 2023, the global textile market was valued at approximately USD 1.7 billion [1], with forecasts projecting steady expansion to around USD 3.05 billion by 2033, driven by a compound annual growth rate of roughly 7.6% [1]. This growth is supported by rising demand across key sectors, including apparel, household textiles, technical textiles, and protective fabrics. Moreover, interest in textile surface modification has increased substantially, as numerous studies have shown that tailored functional finishes can markedly enhance performance by imparting properties such as super-hydrophobicity, antimicrobial activity, self-healing behaviour, flame retardancy, UV shielding, electrical conductivity, and photocatalytic functionality [2–5]. Among the different types of textile, cotton is the most widely used natural textile fibre, and is extensively employed in clothing, household goods, medical, and industrial fields due to its excellent softness, comfort, breathability, high resistance to alkaline conditions, moisture absorption, and renewability [6]. However, cotton is highly hydrophilic because its main component, cellulose, contains many hydroxyl groups. This strong hydrophilicity can promote bacterial growth over extended use, as water trapped within its structure serves as a medium for many microorganisms to thrive. Not only the presence of microorganisms can pose health risks to the user, but it can also result in the textile discoloration, unpleasant odour, and deterioration of mechanical properties [7]. Furthermore, in healthcare, cotton fabrics employed as bed linen, patient gowns, and bandages can become contaminated with various types of body fluids, increasing the risk of

* Corresponding author.
E-mail address: agnese.dagostino@unibg.it (A. D'Agostino).

https://doi.org/10.1016/j.rechem.2026.103615
Received 6 February 2026; Accepted 6 July 2026
Available online 11 July 2026

infection transmission [8]. Therefore, developing durable antibacterial cotton fabrics is crucial for their effective use in healthcare [9–11]. The application of antimicrobial agents to cotton fabrics is broadly divided into three major categories: organic, natural and inorganic materials [12]. The first one, organic materials, includes quaternary ammonium salts, guanidine, peptides, zwitterionic betaine compounds, and halides [13–16]. The second category, which includes natural materials derived from plants or animal sources, such as chitosan derivatives and colourants, has been shown to possess strong antimicrobial activity. Finally, inorganic agents, including nano-ZnO, nano-TiO_2, nano-CeO_2, nano-Ag, and carbon quantum dots, have been studied for their strong antibacterial activity at low concentrations [17–21]. However, conventional treatments often lack durability, necessitating long-lasting antimicrobial finishes that withstand repeated laundering.

Silver nanoparticles (AgNPs) have been found to be an interesting material, due to their remarkable optical, electrical, catalytic, and specifically antimicrobial properties [22–26]. The potent antimicrobial efficacy of AgNPs against a broad spectrum of microorganisms, including bacteria, fungi, and viruses, has led to their widespread adoption in various industrial sectors, such as textiles, food, consumer products, and medicine [26]. Currently, AgNPs are prevalently employed in healthcare products, women's hygiene products, the food industry, paints, cosmetics, medical devices, sunscreens, biosensors, clothing, and electronics. However, increased utilisation of AgNPs-enhanced products may result in elevated toxicity levels, impacting both the environment and living organisms. The antimicrobial activity of AgNPs is primarily attributed to silver ions, which are released from silver-containing compounds and interact with the thiol groups of enzymes and proteins essential for microbial life, disrupting cellular respiration and leading to cell death [27]. Generally, AgNPs are prepared *ex situ* and then physically deposited onto fibers using conventional methods, such as the pad-dry-cure process [7]. However, in this way, AgNPs exhibit low energetic affinity for textiles and could leach from the substrate during use and laundering, with potential adverse effects on humans and the environment. To address this issue, *in situ* synthesis of AgNPs directly onto textiles may be a viable solution [27,28]. Additionally, for biomedical applications, it is recommended that a green and nontoxic synthesis method be employed to mitigate potential biological hazards [29–31]. These nanoparticles are highly effective, offering broad-spectrum antimicrobial activity and a strong capacity to disrupt microbial biofilms.

Polysaccharides, natural macromolecules composed of monosaccharide units linked by glycosidic bonds, can play a crucial role in AgNPs biosynthesis due to their biocompatibility, biodegradability, and diverse biological activities [32–36]. Among them, chitosan, the second most-abundant natural polysaccharide, is particularly notable. Unlike most neutral or acidic polysaccharides, chitosan uniquely exhibits metal-ion chelation, antimicrobial activity, and mucoadhesive properties [32,37–39]. This is due to its polycationic nature, which contains amino groups (NH_2) that strongly bind to metal ions, such as silver ions. According to the literature, Ag^+ ions first interact with the NH_2 groups on the polymer chains [40,41]. Subsequently, the primary and secondary alcohol groups of chitosan are oxidized to aldehydes and ketones, respectively, reducing Ag^+. It is also proposed that the glycosidic bond may play a role in reducing Ag^+, thereby contributing to the formation of a ketone or ester at the glycosidic ring [40]. Therefore, chitosan not only reduces silver ions but also stabilizes the resulting AgNPs by forming hydrogen bonds, electrostatic interactions, and Van der Waals forces between the surface of the nanoparticles and the amino groups of chitosan. Chitosan-stabilized AgNPs can combine the intrinsic properties of both components, often yielding synergistic antimicrobial effects. Chitosan contributes antibacterial activity through electrostatic interactions with negatively charged bacterial surfaces, leading to membrane disruption. [32,42]. For instance, AgNPs have been generated on cotton *via* plasma treatment followed by coating with a silver carbamate complex using a simple *in situ* pad-dry-cure process [28]. Complementarily, chitosan offers a bio-based, dual-function role, serving as a mild reductant for Ag^+ at room temperature and as a stabilizer/ligand *via* amino-group coordination to Ag^0, as elucidated spectroscopically [43]. On cellulose, carboxylic crosslinkers are known to improve the laundering durability of AgNPs finishes [44], albeit without the cationic matrix provided by chitosan [44].

In this study, citric-acid-mediated cellulose functionalization with chitosan-assisted *in situ* generation of AgNPs was used to produce wash-durable antibacterial cotton under mild conditions. The finishing strategy comprises three sequential steps: (i) covalent grafting of citric acid onto cotton cellulose (*via* esterification under pad-dry-cure conditions) to introduce anchored carboxyl functionalities that act as coordination/ion-exchange sites; (ii) impregnation with $AgNO_3$ solution to load Ag^+ within the carboxyl-functionalized fibre network; and (iii) immersion in chitosan solution to promote *in situ* reduction of Ag^+ to Ag^0 and concomitant stabilization of the newly formed AgNPs through chitosan coordination and polymeric capping. Importantly, although thermal curing is required to establish the citric-acid-crosslinked platform, no additional thermal post-treatment is applied to drive the $Ag^+ \rightarrow Ag^0$ conversion, which proceeds at room temperature in the presence of chitosan. To the best of our knowledge, reports combining citric-acid grafting as the Ag^+ binding platform with chitosan as the sole bio-based reducing/stabilizing agent for *in situ* AgNPs formation on cotton remain scarce. This work therefore provides a straightforward route to integrate AgNPs-derived antibacterial functionality against *Staphylococcus aureus* (Gram-positive) and *Escherichia coli* (Gram-negative), with improved laundering durability, making these materials attractive for the production of fabrics for health applications.

2. Experimental

2.1. Materials

Scoured and bleached cotton fabrics (plain woven, 331 g/m^2) were kindly provided by Mascioni SpA (Cuvio, Italy). Prior to all experiments, textile samples were conditioned for 24 h under standard laboratory conditions (65 ± 4% relative humidity and 20 ± 2 °C) to ensure uniform moisture content and temperature. Silver nitrate ($AgNO_3$), citric acid (CA), sodium hypophosphite (SHP), glacial acetic acid, and chitosan with deacetylation grade >75%, medium MW (80 kDa–160 kDa), were purchased from Merck (Milan, Italy) and used as received without further purification.

2.2. Cotton fabrics finishing by chitosan-assisted in situ synthesis of AgNPs

Scoured and bleached cotton fabrics were first carboxyl-functionalized by padding in an aqueous solution containing citric acid (CA, 60 g L^{-1}) and sodium hypophosphite monohydrate (SHP, 70 g L^{-1}) using a two-roll laboratory padder (nip pressure 3 bars; wet pick-up 70%). The padded samples were dried at 80 °C for 3 min and cured at 150 °C for 5 min to promote CA cellulose esterification and generate a carboxyl-functionalized cotton platform. For Ag^+ loading, carboxyl-functionalized specimens (5 cm × 5 cm) were immersed in $AgNO_3$ aqueous solutions (0.01 M or 0.1 M) for 2 h at 20 °C. The $AgNO_3$ uptake step was conducted under excess-bath conditions to avoid Ag^+ depletion; the liquor ratio (fabric mass to solution volume) was 1:25, corresponding to approximately 20 mL per 5 cm × 5 cm specimen. The resulting samples were denoted CA_Ag001 and CA_Ag01, respectively, according to the $AgNO_3$ concentration used. Ag^+ loaded fabrics were then transferred into chitosan solutions to induce *in situ* reduction and stabilization. Chitosan solutions (1% or 3% w/w) were prepared by dissolving chitosan in dilute acetic acid under stirring at 60 °C for 3 h, followed by cooling to room temperature. The fabrics were incubated in the chitosan bath at room temperature for 2 h to allow reduction and particle maturation. The treatment was carried out at a liquor ratio (fabric mass to solution volume) of 1:40. The samples were then

thoroughly rinsed with double-distilled water (18.2 MΩ·cm) to remove loosely bound species, and finally dried at 60 °C for 72 h prior to characterization. A schematic representation of the cotton fabric finishing process is presented in Scheme 1.

2.3. Washing fastness of treated fabrics

The washing fastness test of the treated fabrics was conducted in accordance with ISO 105-C10:2006 [45]. Accordingly, textile samples were washed at 40 °C for 30 min in an aqueous solution containing a neutral commercial detergent (2.0 g L^{-1}) at a material-to-liquor ratio of 1:30, using a Labomat (Werner Mathis, Zurich, Switzerland). Subsequently, they were gently squeezed and rinsed with tap water and finally dried overnight at room temperature. This procedure was repeated 1, 5, and 10 times to obtain samples corresponding to 1, 5, and 10 washing cycles. The prepared samples were stored in a dark environment under atmospheric pressure at 20 ± 1 °C and 65 ± 2%RH before all experiments, as a standard procedure for textile materials. The samples were coded according to the chemical treatments and concentrations applied, as summarized in Table 1. For each formulation, one portion was kept unwashed, while the remaining portions were subjected to the scheduled washing cycles.

2.4. Characterization techniques

Colour differences between treated and untreated textile samples were evaluated after each synthetic step and using a Datacolor Spectro 700 spectrophotometer (Datacolor, Italy). This instrument enables the quantification of colour variation (ΔE*) based on CIE L*a*b* coordinates, where L*, a*, and b* represent lightness, red/green, and yellow/blue components, respectively, by comparing each sample to a reference standard, applying the formula in Eq. (1):

$$\Delta E^{*} = \sqrt{(\Delta L^{*})^{2} + (\Delta a^{*})^{2} + (\Delta b^{*})^{2}} \quad (1)$$

where ΔL*, Δa*, and Δb* are the differences in lightness, in a* and b* values, respectively.

K/S values were determined based on the results of tests performed on the Datacolor Spectro 700 spectrophotometer reflection spectrometer in the following conditions: colour system CIE L*a*b*, light D65, observation angle 10°.

Changes in the morphology and elemental composition of both untreated and treated fabric samples were examined using a scanning electron microscope (SEM; Phenom ProX G6 Desktop SEM, Thermo Fisher Scientific, Italy), operated at 15 kV in backscattered electron (BSE) mode and equipped with an energy-dispersive X-ray spectroscopy (EDX) detector.

Chemical surface modifications induced by the finishing treatment before and after were investigated using a Thermo Avatar 370 FTIR spectrometer (Thermo Nicolet Corp., Madison, WI, USA), equipped with a diamond attenuated total reflection (ATR) accessory. For each sample, three replicate spectra were acquired in absorbance mode over the range of 4000–700 cm^{-1}, averaging 32 scans at a resolution of 4 cm^{-1}. The resulting spectra were normalized to the 1315 cm^{-1} band assigned to CH_2 wagging of cellulose, located in a spectral region unaffected by the finishing treatment. Spectral analysis was carried out using Omnic software (v7.3), and data processing was performed with Origin (v7.0).

Raman spectroscopy was performed on the fabrics using an XploRA Plus Raman spectrometer (HORIBA Scientific, Kyoto, Japan) equipped with a 600 groove/mm diffraction grating and integrated with an Olympus confocal microscope. Spectra were acquired over the 150–3900 cm^{-1} range using a 785 nm excitation laser (100 mW) focused on the sample through a 100× objective lens (numerical aperture 0.9). For each sample, three measurements were performed to ensure reproducibility, with spectra collected over an integration time of 100 s and

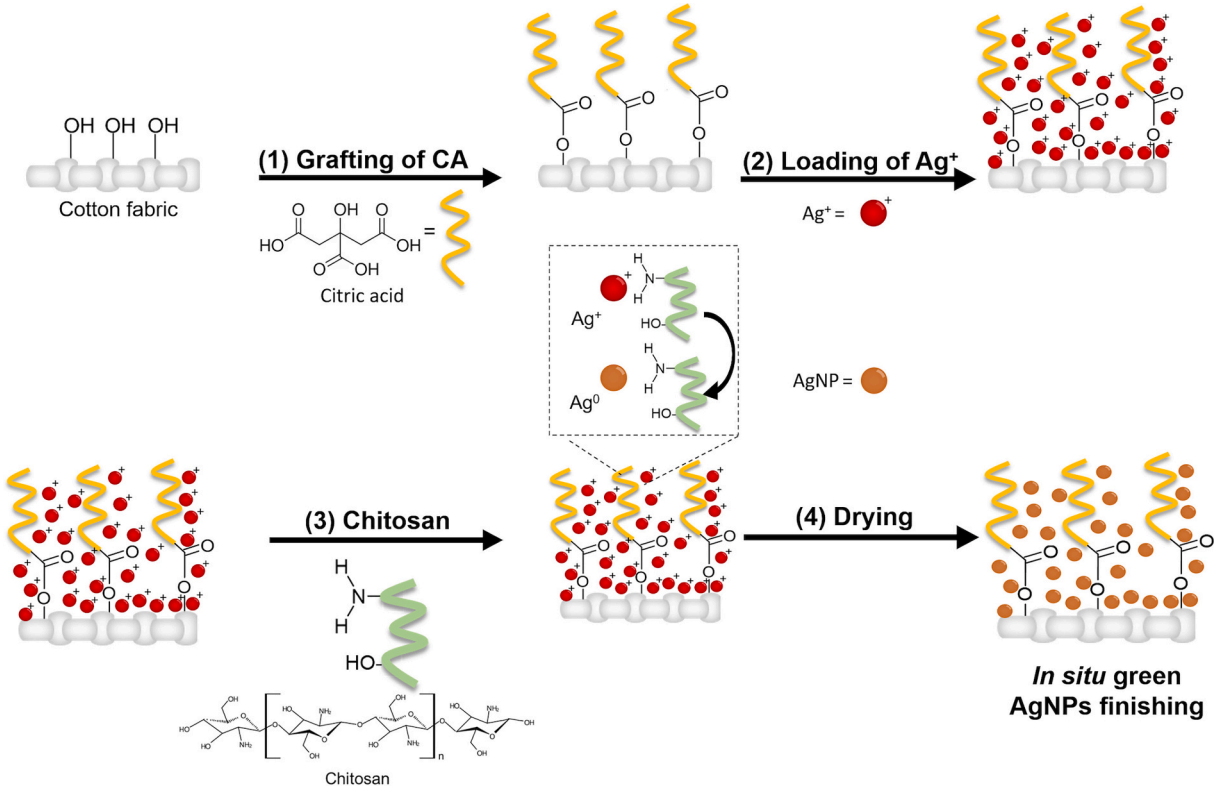

Scheme 1. Schematic illustration of the *in situ* green synthesis route for AgNPs-functionalized cotton fabrics, depicting the successive stages of citric acid grafting, silver ions loading, and chitosan treatment.

Table 1
Experimental synthesis parameters and identification codes of the prepared samples.

Sample code	$AgNO_3$ loading (M)	Chitosan treatment (% w/w)	1 W	5 W	10 W
CA_Ag001_C1	0.01	1	CA_Ag001_C1 1W	CA_Ag001_C1 5W	CA_Ag001_C1 10W
CA_Ag001_C3	0.01	3	CA_Ag001_C3 1W	CA_Ag001_C3 5W	CA_Ag001_C3 10W
CA_Ag01_C1	0.1	1	CA_Ag01_C1 1W	CA_Ag01_C1 5W	CA_Ag01_C1 10W
CA_Ag01_C3	0.1	3	CA_Ag01_C3 1W	CA_Ag01_C3 5W	CA_Ag01_C3 10W

CA: citric acid-grafted cotton; Ag001 and Ag01 indicate samples loaded using 0.01 M and 0.1 M aqueous $AgNO_3$ solutions, respectively; C1 and C3 indicate samples treated with 1% and 3% w/w chitosan solutions, respectively; W: washing cycles.

an accumulation of 2. The most representative spectra were selected for analysis and presentation. Baseline correction was applied to all spectra, followed by min-max normalization.

Mechanical properties were assessed in terms of maximum force (N) and elongation at break (%) in the weft and warp directions, according to ISO 13934-1:2013 (strip method) 2013 [46], with minor modifications, using a Z005TH ProLine 5kN testing machine (ZwickRoell GmbH, Ulm, Germany). Specimens were prepared as rectangular strips (15 mm × 50 mm) and conditioned at 20 ± 2 °C and 65 ± 5% relative humidity for 24 h prior to testing. Tensile tests were performed at a constant crosshead speed of 100 mm·min^{-1} with a clamp spacing of 30 mm, using five replicates per direction. Results are reported as mean ± standard deviation. Statistical comparisons were conducted using one-way ANOVA followed by Tukey's multiple-comparisons *post hoc* test ($\alpha = 0.05$).

The total silver (Ag) content in the treated fabrics was determined by inductively coupled plasma mass spectrometry (ICP-MS), in accordance with UNI EN ISO 16711-1:2015 and UNI EN ISO 17294-2:2023. For ICP-MS, the calibration range, internal standard, and LOD/LOQ were reported along with details of sample acid digestion and recovery. A mass-balance assessment (textile Ag retained *vs.* Ag released to wash liquor) is provided to complement EDX semi-quantification. Following established practice for AgNPs-textile systems, distinguishing between ionic dissolution and particulate release is essential for durability claims. Prior to analysis, samples were digested by microwave-assisted mineralization using 68% nitric acid (HNO_3) to ensure complete dissolution of the matrix. To quantify silver (Ag) in the washing waters collected after 1, 5, and 10 washing cycles, 20 mL of sample were acidified with 5 mL of nitric acid (HNO_3) and subjected to microwave-assisted digestion at 170 °C for 10 min, following the UNI EN ISO 15587-2:2022 standard for sample digestion. After mineralization, the solutions were appropriately diluted and analysed by ICP-MS in accordance with UNI EN ISO 17294-2:2023 for quantitative determination.

UV–vis spectra of washing water were recorded on a UV–vis absorption spectrophotometer (Thermo Nicolet Evolution UV–vis-500, Waltham, MA, USA) in the range of 200–800 nm, using a 1 cm pathlength cell. All spectra were acquired at room temperature.

2.5. Antibacterial assay

The antibacterial performance of untreated cotton (UT), citric-acid-treated cotton (CA), and Ag/chitosan-functionalized samples (CA_Ag001_C1, CA_Ag001_C3, CA_Ag01_C1, CA_Ag01_C3) was evaluated against *Staphylococcus aureus* (ATCC 6538, Gram-positive) and *Escherichia coli* (ATCC 11229, Gram-negative), following the ASTM E2149-13a "Standard test method for determining the antimicrobial activity of immobilized antimicrobial agents under dynamic contact conditions", with minor modifications [47]. UT and CA were evaluated in the unwashed state, whereas Ag/chitosan-functionalized samples were evaluated both before washing and after 5 and 10 washing cycles. The incubated test culture in a nutrient broth was diluted to give a concentration of 1.5–3.0 × 10^5 CFU mL^{-1} (working dilution) as determined by spectrophotometric analysis at OD_{475}. Square cotton specimens (2 cm × 2 cm, ≈ 0.25 g) were placed in 50 mL Falcon tubes containing 12.5 mL of the working solution. Samples were incubated for 1 h at room temperature under stirring to ensure dynamic contact. After contact, aliquots of the bacterial suspension were serially diluted (10^3-fold), plated on Yeast Extract Agar (Sigma-Aldrich), and incubated at 37 °C for 24 h. The number of surviving colonies (CFU mL^{-1}) was determined using the plate count method. The antibacterial efficacy was expressed as a percentage reduction relative to the control according to Eq. (2):

$$\%bacterial\ reduction\ \left(CFU.mL^{-1}\right) = \frac{B-A}{B} \times 100 \quad (2)$$

where A is the CFU mL^{-1} after exposure to the test specimen and B is the CFU mL^{-1} of the initial bacterial inoculum (growth control).

The antibacterial assay was based on a dynamic-contact protocol followed by serial dilution, agar plating, incubation, and CFU enumeration. The bacterial reductions reported in Fig. 6 were calculated from plate-count data obtained from triplicate independent experiments. To improve transparency, the corresponding quantitative antibacterial reduction values are provided in **Table S1** for both *S. aureus* and *E. coli*. UT and CA were not subjected to laundering; in particular, CA represents the citric-acid-functionalized intermediate sample used for subsequent Ag loading and Ag/chitosan functionalization. Therefore, post-washing antibacterial reduction values are not reported for these samples. Representative agar plate images are provided in **Fig. S3** for selected *S. aureus* samples as visual examples of the microbiological assay. Since ASTM E2149-13a is a suspension-based dynamic-contact method, inhibition-zone measurements were not performed, as they are associated with agar diffusion assays and evaluate a different antimicrobial mechanism. All tests were performed in triplicate using independent bacterial cultures.

Data are expressed as mean ± standard deviation (SD). Statistical significance was assessed using a one-way ANOVA with Tukey's correction, with $p < 0.05$ considered significant. Statistical analyses were performed with GraphPad Prism version 6 (GraphPad Software, La Jolla, CA, USA).

3. Results and discussion

3.1. Colorimetric properties and surface morphology

To evaluate the effect of the different finishing steps on surface optical properties, the CIE L*a*b* colour coordinates and K/S values of untreated and treated cotton fabrics were analysed (Table 2). The CIE-LAB parameters provide quantitative descriptions of lightness (L*) and chroma along the red-green (a*) and yellow-blue (b*) axes, whereas the K/S values, derived from the Kubelka-Munk function, are commonly used as indicators of colour strength and surface optical density.

The untreated control sample (UT) exhibited very high lightness (L* = 95 ± 0.5) and low chromaticity values (a* = −0.51 ± 0.3, b* = 2.91 ± 0.3), indicating a nearly neutral white appearance with a slight yellowish tint. A similar profile was observed for CA (L* = 95 ± 0.2), although a more noticeable yellow hue (b* = 5 ± 0.2) and green component (a* = −1 ± 0.2) were present. The K/S value for CA was 0.08 ± 0.01, suggesting a very low level of yellow coloration. This could be ascribed to the formation of aconitic acid during the grafting of citric acid [48,49]. Upon loading with silver ions at a concentration of 0.01 M

Table 2
CIE L*a*b colour coordinates and K/S values for the untreated cotton (UT), citric acid-grafted sample (CA), and the series of samples subjected to silver ions loading followed by chitosan treatments with different concentrations (CA_Ag001, CA_Ag001_C1, CA_Ag001_C3, CA_Ag01, CA_Ag01_C1, CA_Ag01_C3).

Sample code	Sample image	L*	a*	b*	K/S
UT		95 ± 0.5	−0.51 ± 0.3	2.91 ± 0.3	0.04
CA		95 ± 0.2	−1 ± 0.2	5 ± 0.2	0.08 ± 0.01
CA_Ag001		69 ± 4	8 ± 2	26 ± 4	1.5 ± 0.7
CA_Ag001_C1		64 ± 4	10 ± 2	32 ± 3	2.6 ± 0.5
CA_Ag001_C3		74 ± 3	7 ± 1	31 ± 2	1.6 ± 0.4
CA_Ag01	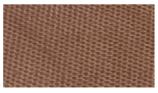	37 ± 2	11 ± 3	16 ± 3	8.5 ± 1.2
CA_Ag01_C1		46 ± 4	30 ± 6	30 ± 7	9.1 ± 1.2
CA_Ag01_C3		49 ± 4	15 ± 1	20 ± 3	6.6 ± 1.4

(CA_Ag001), a significant reduction in lightness was observed (L* = 69 ± 4), accompanied by a marked increase in redness (a* = 8 ± 2) and yellowness (b* = 26 ± 4). This shift was further intensified with the addition of chitosan. In particular, the sample CA_Ag001_C1 showed further darkening (L* = 64 ± 4) and a strong increase in chromaticity (a* = 10 ± 2, b* = 32 ± 3), with an associated K/S value of 2.6, indicating a higher optical density [48,49]. CA_Ag001_C3 displayed a slightly higher lightness (L* = 74 ± 3), but retained elevated chromatic values (a* = 7 ± 1, b* = 31 ± 2) and a K/S of 1.6. A much more pronounced effect was observed at the silver ions concentration of 0.1 M (CA_Ag01), where lightness dropped sharply (L* = 37 ± 2) and chromaticity increased notably (a* = 11 ± 3, b* = 16 ± 3), resulting in the highest K/S value recorded (8.5 ± 1.2) [42]. When combined with chitosan, the CA_Ag01_C1 sample exhibited a substantial enhancement of the red and yellow components (a* = 30 ± 6, b* = 30 ± 7), with a corresponding K/S value of 9.1, indicating intense coloration and significant surface interaction. The CA_Ag01_C3 sample exhibited a slightly lighter tone (L* = 49 ± 4) and lower a* and b* values (a* = 15 ± 1, b* = 20 ± 3), though still maintained a high K/S (6.6). These findings demonstrate that both the loading of silver ions and the treatment with chitosan strongly influence the optical and colorimetric properties of the treated fabrics, with chitosan enhancing dye uptake and visual intensity, particularly at higher silver content [49]. The finishing process induced a clear and formulation-dependent colour modification. As shown by the decrease in L* and the increase in K/S (Table 2), higher $AgNO_3$ loading and chitosan treatment led to darker and more intensely colored fabrics. Overall, the colourimetric data demonstrate a clear formulation-dependent optical response, governed primarily by silver loading and modulated by chitosan concentration. The progressive decrease in lightness and increase in K/S with increasing $AgNO_3$ concentration and chitosan treatment are consistent with the presence of Ag-based nanostructures on the fibre surface, which modify optical properties through absorption and scattering effects. From an application perspective, such colour changes may be acceptable or even advantageous for technical, medical, and protective textiles, while they could limit use in applications requiring high whiteness.

Although noticeable colour changes were observed, including a pronounced shift toward yellow, colourimetric data alone are insufficient to confirm the formation of AgNPs. Consequently, scanning electron microscopy (SEM) was employed to investigate surface morphology and assess the presence of AgNPs. SEM images of untreated and treated fabrics are reported in Fig. 1.

The SEM micrograph of the untreated cotton fibre reveals a characteristic smooth surface, featuring longitudinal fibrils and bundles. Treatment with silver ions alone does not induce any noticeable change in the fibre morphology, which remains comparable to that of the pristine material. However, after the subsequent chitosan-mediated reduction step, SEM analysis reveals the formation of uniformly distributed silver-containing particles, hereafter described as Ag-rich surface domains, on the fibre surface. These Ag-rich surface domains display a predominantly spherical morphology. For each sample type, the reported mean diameters and standard deviations were calculated from at least 60 SEM-visible particles, measured from two independent SEM images, with at least 30 particles analysed per image. The average diameters of the SEM-visible Ag-rich domains were determined to be (356 ± 18) nm and (282 ± 28) nm for CA_Ag001_C1 and CA_Ag001_C3, respectively. Upon increasing the silver precursor concentration, a modest rise in the mean domain size was observed reaching (358 ± 37) nm for CA_Ag01_C1 and (295 ± 40) nm for CA_Ag01_C3. In the SEM images, the observed Ag-rich features have submicron mean diameters (≈0.28–0.36 μm); to avoid ambiguity with the conventional <100 nm definition of nanoparticles, these features are referred to here as submicron Ag-containing particles or AgNP aggregates, without inferring a primary crystallite size. At lower silver ion concentrations, a high density of smaller, well-dispersed Ag-rich domains is observed, whereas at higher silver concentrations, the number of SEM-visible Ag-rich domains is reduced and the size distribution becomes broader. This trend suggests that when an excess of silver ions is present, aggregation or fewer effective nucleation events may occur due to saturation of the available chitosan functional groups for reduction and stabilization. These observations strongly support an *in situ* synthesis mechanism, highlighting the critical role of chitosan in governing the density and distribution of Ag-rich domains while maintaining the integrity of the cotton fibers.

Scanning electron microscopy (SEM) coupled with energy-dispersive X-ray (EDX) analysis was employed to provide a comprehensive qualitative characterization of the Ag/chitosan-functionalized fabrics. The changes in elemental composition between untreated and treated samples, resulting from the *in situ* formation of Ag-containing domains, are presented in **Fig. S1**. The EDX analysis of untreated cotton (UT) exhibited carbon (C) and oxygen (O) signals, consistent with the cellulose structure of the fibers. Upon grafting citric acid onto the cotton fibers (CA), an increase in the presence of sodium (Na) and phosphorus (P) was observed, indicating the incorporation of these elements from the catalyst used during the crosslinking reaction. Specifically, SHP was used as a catalyst to promote grafting and enhance the functional properties of the treated fabrics [50]. Following silver (Ag) treatment, a distinct silver (Ag) signal was observed in EDX analysis, with an

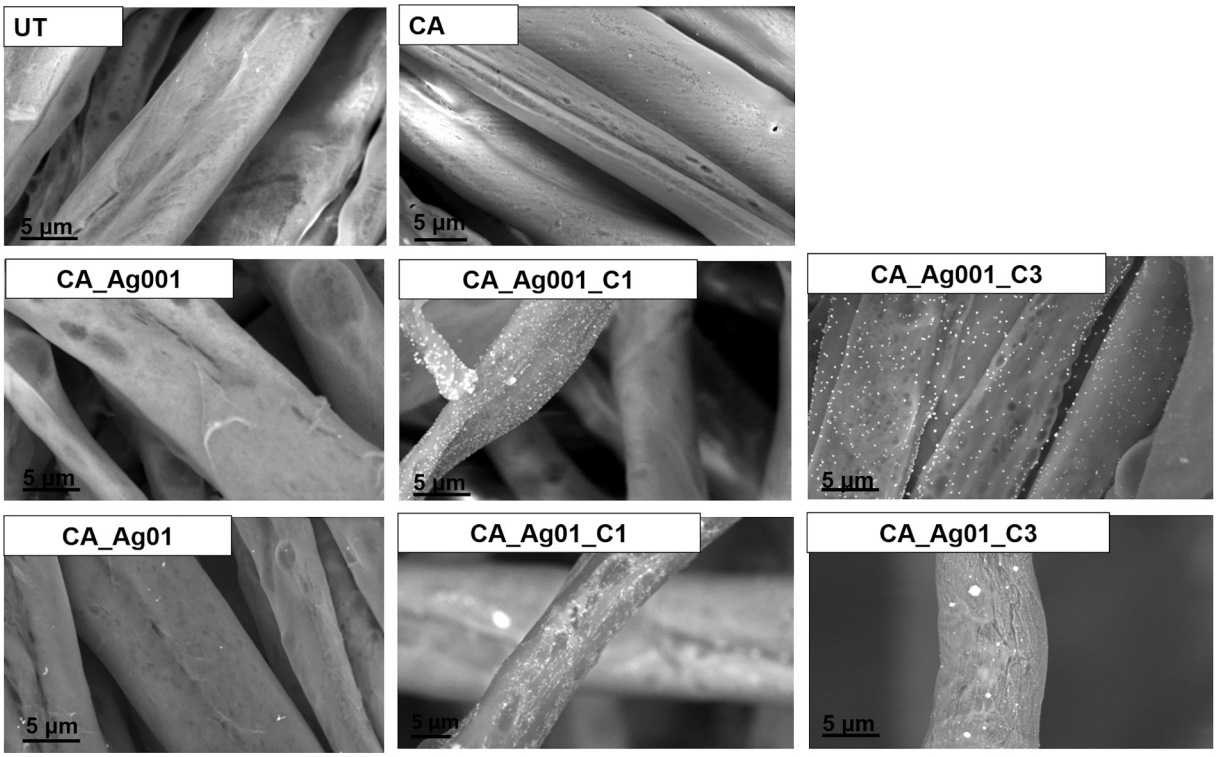

Fig. 1. SEM micrographs (10,000× magnification) of the untreated cotton (UT), the citric acid-grafted sample (CA), and the series of fabrics functionalized through silver ion loading followed by chitosan treatments at varying concentrations (CA_Ag001, CA_Ag001_C1, CA_Ag001_C3, CA_Ag01, CA_Ag01_C1, CA_Ag01_C3).

intensity correlating with the amount of silver applied (CA_Ag001; CA_Ag01), confirming successful deposition of silver on the cotton surface [51]. Following chitosan treatment, increases in carbon (C) and oxygen (O) signals were observed, whereas the silver (Ag) signal decreased. This can be attributed to the deposition of a chitosan layer over the cotton surface, which is rich in carbon and oxygen due to its polysaccharide structure [51]. Overall, these EDX findings provide valuable insights into the elemental changes occurring on cotton fibers during the functionalization process, highlighting the roles of citric acid, silver, and chitosan at each synthetic step.

3.2. *Spectroscopic investigation*

To confirm the surface chemical modifications induced by the sequential treatments outlined in Scheme 1, ATR-FTIR spectroscopy was employed. The ATR mode was selected to minimize scattering artefacts arising from the intrinsic roughness and fibrous morphology of cotton substrates, which often compromise spectral quality in transmission measurements. Fig. 2 compares the FTIR spectra of untreated cotton (UT), citric-acid-grafted cotton (CA), and samples subjected to sequential Ag^+ loading and chitosan treatments.

The spectrum of untreated cotton displays the characteristic broad O—H stretching band centered at ~3332 cm^{-1}, together with C—H stretching vibrations in the 2980–2800 cm^{-1} region and bands at 1433–1428 cm^{-1} and ~ 1028 cm^{-1} associated with cellulose C—H deformation and C—O stretching modes, respectively [52]. A band at ~1637 cm^{-1} is attributed to the bending vibration of adsorbed water molecules, commonly observed in cellulosic materials. Following citric acid treatment, the appearance of a distinct absorption band at ~1720 cm^{-1} is observed, which is assigned to ester C═O stretching vibrations. This feature provides clear evidence of ester bond formation between citric acid and cellulose hydroxyl groups, consistent with polycarboxylic-acid-based durable-press finishing of cotton under pad-dry-cure conditions [49]. The esterification process is known to proceed through thermally generated anhydride intermediates in the

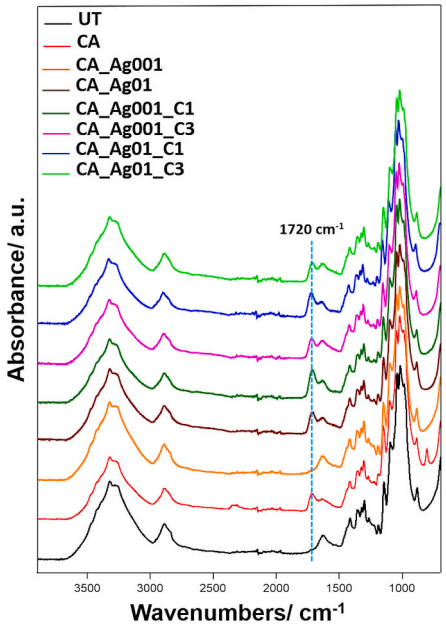

Fig. 2. FTIR spectra of untreated cotton (UT), citric acid-grafted fabric (CA), and the series of samples functionalized *via* sequential silver ion loading and chitosan treatments conducted at varying concentrations (CA_Ag001, CA_Ag001_C1, CA_Ag001_C3, CA_Ag01, CA_Ag01_C1, CA_Ag01_C3).

presence of sodium hypophosphite, leading to covalent grafting while leaving a fraction of carboxyl groups unreacted and anchored to the fibre surface. Upon Ag^+ loading, partial attenuation of the 1720 cm^{-1} band is observed for samples treated with lower silver concentrations, which can be rationalized by coordination interactions between Ag^+ ions and CA-derived carboxylate/oxygen donor groups. At higher Ag^+

concentrations, the persistence of this band suggests that not all ester or carboxyl functionalities participate in silver coordination, indicating an excess of available binding sites within the CA-modified fibre matrix. Subsequent treatment with chitosan results in a modest decrease in the intensity of the broad O—H stretching region (3500–3000 cm^{-1}), consistent with the formation of a thin chitosan-based coating and enhanced hydrogen-bonding interactions at the fibre surface. Importantly, the ester carbonyl band at ~1720 cm^{-1} remains detectable in all chitosan-treated samples, indicating that the CA-induced ester network is preserved during Ag^{+} reduction and nanoparticle formation. Overall, the FTIR results support a mechanism in which Ag^{+} ions are initially coordinated at CA-functionalized sites and subsequently reduced *in situ* in the presence of chitosan, which concurrently acts as a stabilizing and capping polymer. Chitosan-mediated reduction of Ag^{+} to reduced silver species/Ag(0) in aqueous chitosan systems has been reported in previous mechanistic studies, including evidence based on UV-Vis and XPS analyses for reduced silver formation and concomitant oxidation of chitosan functionalities [43]. Other studies on chitosan-based AgNPs formation further support the ability of chitosan to act as both reducing and stabilizing agent under mild aqueous conditions [53,54]. In the present work, the reduction pathway is therefore discussed as plausible and literature-supported, while acknowledging that the present characterization set primarily evidences Ag incorporation and Ag-rich particle formation on cotton rather than providing full oxidation-state quantification. Based on the present experimental evidence and literature reports, this process can be tentatively summarized schematically as:

$$2\,Ag^{+} + Chit \rightarrow 2\,Ag^{0}@Chit + Chit_{ox} + 2H^{+}$$

where $Chit_{ox}$ denotes partially oxidized chitosan moieties.

The persistence of ester carbonyl features after Ag/chitosan functionalization is therefore consistent with a surface-mediated reduction mechanism, in which chitosan facilitates Ag^{+} reduction and nanoparticle stabilization without disrupting the underlying CA-cellulose ester framework.

Raman spectroscopy provides complementary evidence consistent with Ag-ligand interactions at the fibre surface: a low-frequency feature near ~140 cm^{-1}, absent in untreated cotton, is compatible with vibrational modes involving Ag—O or Ag—N interactions. This Raman feature is treated here as supportive evidence only, while Ag-containing particle formation and retention are primarily evidenced by SEM/SEM-EDX and quantitative Ag analysis by ICP-MS. This supports the hypothesis of silver anchoring or coordination to the fibre surface induced by chitosan treatment [55], as reported in Fig. 3.

Raman measurements of the modified cotton fibers were performed using near-infrared excitation (785 nm), which is advantageous because it minimizes fluorescence interference from the cellulose matrix. In the unmodified cotton (UT), the Raman spectrum is dominated by characteristic cellulose vibrational bands: CCC ring deformation modes (~381, 437, 460 cm^{-1}), CH skeletal rotation (~906 cm^{-1}), C—O—C glycosidic linkage modes (~520 cm^{-1}), and symmetric/asymmetric C—O—C stretching (~1099 and 1126 cm^{-1}) [56]. These same cellulose-derived bands are also observed, albeit with modified intensities or slight shifts in the treated fibers (CA_Ag001_C3, CA_Ag01_C3), indicating that the core cellulose structure remains largely intact after Ag/chitosan functionalization. Meanwhile, the low-frequency feature at ~140 cm^{-1} is compatible with silver-chitosan interactions. The low-frequency Raman response is compatible with metal-ligand modes involving Ag—N/Ag—O, supporting the view that chitosan may contribute to the surface coordination and stabilization of Ag-containing domains on the cotton substrate [42]. In line with prior reports on AgNPs-functionalized cotton at low loadings, where XRD signals of Ag can be weak or absent, the convergence of SEM-EDX, FTIR/Raman, and quantitative Ag analysis is considered sufficient to support Ag incorporation, Ag-rich domain formation, and binding on the cellulosic substrate [27].

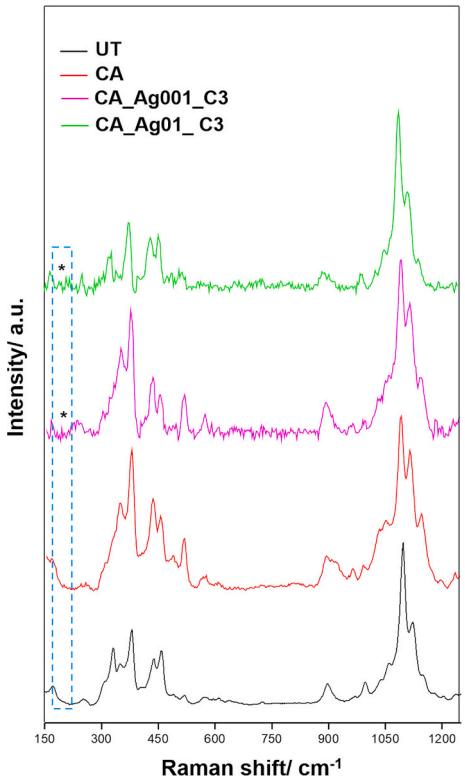

Fig. 3. Raman spectra of untreated cotton (UT), citric acid-grafted fabric (CA), CA_Ag001_C3, CA_Ag01_C3 samples.

3.3. Mechanical performance

As shown in Fig. 1–3, the applied finishing did not cause evident fibre damage in SEM images and did not affect the characteristic cellulose spectroscopic fingerprints observed by FTIR and Raman spectroscopy, indicating that the cotton fibre morphology and chemistry were largely preserved. To assess the mechanical performance of the fabrics, comprehensive mechanical testing was performed, and the results are reported in Table 3.

The untreated cotton (UT) exhibited a maximum force at break of 210 ± 12 N and an elongation at break of 23.9 ± 0.8% in the warp direction, and 151 ± 7 N with 15.3 ± 0.8% in the weft direction. Upon citric-acid treatment (CA), both parameters decreased markedly in both directions (to 113 ± 11 N and 16.6 ± 0.6% in warp; 98 ± 9 N and 11.8 ± 0.4% in weft), corresponding to strength retentions of approximately 54% (warp) and 65% (weft) relative to UT. Such reductions are consistent with reports on polycarboxylic-acid durable-press finishes on cellulosic fabrics, where strength losses are commonly associated with acid-driven cellulose degradation and the formation of ester crosslinks, and are strongly influenced by curing severity and solution acidity

Table 3
Mechanical properties of untreated and treated cotton fabrics in the warp and weft directions: maximum force (N) and elongation at break (%) (mean ± SD; n = 5).

Sample	Warp		Weft	
	Maximum force (N)	Elongation at break (%)	Maximum force (N)	Elongation at break (%)
UT	210 ± 12	23.9 ± 0.8	151 ± 7	15.3 ± 0.8
CA	113 ± 11	16.6 ± 0.6	98 ± 9	11.8 ± 0.4
CA_Ag01_C3	124 ± 5	17.4 ± 0.3	86 ± 7	11.8 ± 0.9
CA_Ag001_C3	130 ± 9	17.9 ± 0.7	98 ± 10	12.9 ± 0.6
CA_Ag01_C1	121 ± 22	20.0 ± 0.3	109 ± 9	14.1 ± 0.5
CA_Ag001_C1	118 ± 7	17.2 ± 0.5	108 ± 11	13.1 ± 0.6

[57,58]. Notably, subsequent Ag/chitosan functionalization did not cause further systematic deterioration beyond the CA-grafted baseline: across the Ag and chitosan formulations investigated, the warp maximum force at break remained within 118–130 N, with the elongation at break ranging from approximately 17.2% to 20.0%, while weft values ranged from 86 to 109 N, with elongation at break of approximately 11.8% to 14.1%. This trend aligns with surface functionalization, in which the coating step produces only minor or statistically non-significant changes in breaking force and elongation under mild processing conditions [59]. In this respect, the largely preserved mechanical performance suggests a predominantly surface-deposited coating governed by non-covalent interactions, rather than covalent esterification-driven crosslinking between the finishing agents and cellulose hydroxyl groups. Overall, the data indicate that the curing step is the dominant contributor to the observed decrease in mechanical properties, whereas Ag incorporation and the chitosan-related treatments have a limited additional impact on fabric integrity within the investigated formulation window.

3.4. Washing durability and silver retention

The washing fastness of the treated samples was evaluated in accordance with ISO 105-C10:2006. Samples were subjected to 1, 5, and 10 washing cycles to assess both the overall durability of the coating and the retention of the Ag-containing fraction on the fabric surface. SEM-EDX analyses of the treated fabrics following different washing cycles are presented in Fig. 4.

Morphological analysis confirmed the persistence of Ag-containing surface domains even after successive washing steps, indicating that a substantial Ag-containing fraction remains associated with the substrate. EDX analysis revealed a gradual decrease in silver content with each wash, particularly in samples initially prepared with higher silver concentrations. To investigate this reduction, the total silver content on the treated samples and the amount released during washing were quantified using ICP-MS. The silver (Ag) loadings measured in the functionalized cotton fabrics ranged from 1.0 to 4.3 mg/g, specifically 1.7 mg/g and 1.0 mg/g for samples CA_Ag001_C1 and CA_Ag001_C3, respectively, and 4.3 mg/g and 3.6 mg/g for CA_Ag01_C1 and CA_Ag01_C3. These values are higher than those reported in previous studies, in which even relatively modest Ag contents (~0.117 mg/g) were sufficient to achieve bacterial reductions exceeding 98% against *S. aureus* and *E. coli*. Moreover, cotton fabrics containing approximately 0.18 mg/g Ag have been shown to reduce bacterial growth by ~99.99% against both bacterial strains. The *in situ*-formed Ag-containing domains, generated *via* an aqueous, room-temperature, chitosan-assisted route that avoids harsh reducing agents, confer antibacterial properties on treated cotton samples. The combination of chitosan and Ag-containing species/domains has been shown to significantly enhance the antibacterial activity of cotton fabrics against both *S. aureus* and *E. coli*. However, it is crucial to note that the relationship between silver content and antibacterial efficacy is not linear. Beyond a certain threshold, increasing silver loading may lead to diminishing returns due to factors such as nanoparticle aggregation, reduced release of Ag^{+} ions, and potential cytotoxicity [60]. Mechanistically, under dynamic-contact antibacterial conditions, the relevant parameter is not the total Ag content on the fabric, but the availability and release of bioactive silver species (predominantly Ag^{+} generated *via* surface oxidation/dissolution). Once this availability exceeds an efficacy threshold, further increases in total Ag loading may not result in proportional improvements in antibacterial activity, leading to a diminishing-returns regime [61]. In addition, SEM observations suggest broader Ag-rich domains at higher precursor concentrations, consistent with aggregation phenomena that reduce the effective surface area per unit Ag mass and limit the accessibility of active sites. Finally, laundering is expected to preferentially remove weakly bound silver during early cycles, while the strongly anchored fraction retained after repeated washing is more representative of long-term antibacterial performance. Considering the present Ag loadings, one can reasonably anticipate very high antibacterial performance, potentially approaching complete bacterial inactivation under suitable contact conditions. Moreover, the form of silver, whether nanoparticulate or ionic, its binding to the substrate, and its durability through laundering cycles are critical determinants of sustained antibacterial performance [62].

The released silver (Ag) detected in the washing water after 1, 5, and 10 cycles for the four sample types is presented in Fig. 5.

Notably, the highest silver release was observed in the CA_Ag01_C1 sample, with concentrations of 13 mg L^{-1} after 1 wash, decreasing to 0.48 mg L^{-1} after 10 washes. Conversely, the CA_Ag001_C3 sample

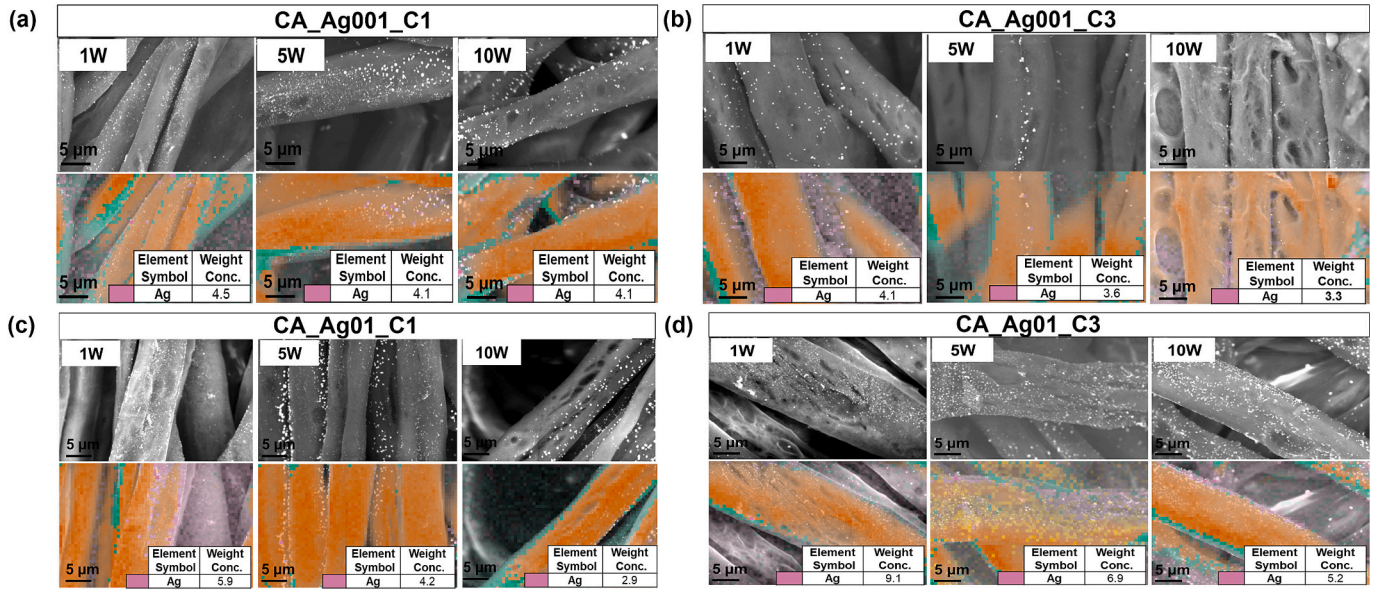

Fig. 4. Combined SEM-EDX analyses of the functionalized cotton fabrics after 1, 5, and 10 washing cycles, illustrating morphological features and silver (Ag) elemental distributions in: (a) CA_Ag001_C1; (b) CA_Ag001_C3; (c) CA_Ag01_C1; (d) CA_Ag01_C3. In the elemental maps, silver (Ag) is visualized in pink, whereas carbon (C) and oxygen (O) are rendered in orange and green, respectively. (For interpretation of the references to colour in this figure legend, the reader is referred to the web version of this article.)

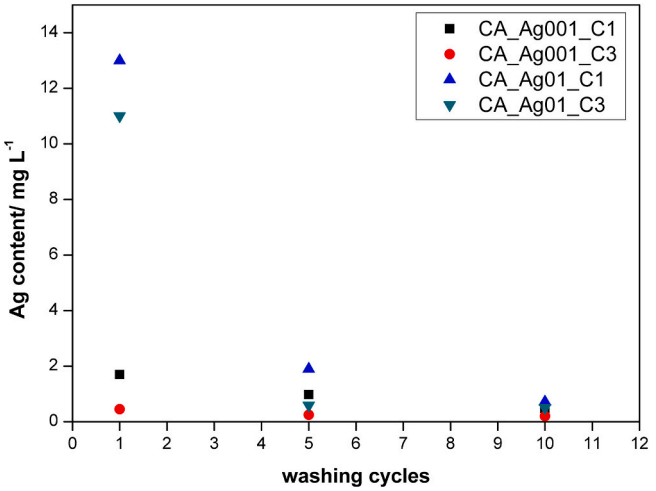

Fig. 5. Silver released into washing water over 1, 5, and 10 cycles for Ag/chitosan-functionalized cotton samples (CA_Ag001_C1, CA_Ag001_C3, CA_Ag01_C1, CA_Ag01_C3).

exhibited lower initial silver release, with values of 0.45 mg L^{-1} after 1 wash, declining to 0.20 mg L^{-1} after 10 washes. These results align with a previous study in which silver concentrations in washing effluents ranged from 0.1 to 1.3 mg L^{-1}, depending on the type of textile and the presence of AgNPs [63]. Over successive washing cycles, the silver concentration decreases, indicating a progressive reduction in the amount of readily releasable Ag species, possibly due to the removal of weakly bound silver during the first washing steps. Differences in silver release among the sample types may be attributed to variations in the binding strength of Ag-containing species/domains to the cotton fibers, influenced by factors such as chitosan concentration and silver loading. Overall, although initial silver concentrations in the washing effluents are relatively high, the gradual decrease over multiple wash cycles suggests progressive depletion of weakly bound or readily releasable Ag species. Interpreting wash-off involves differentiating Ag^+ dissolution from the release of particulate Ag-containing species. According to previous studies [27], ICP-based mass balances provide quantitative information on total Ag wash-off, whereas UV–vis spectra of wash liquors can provide only limited qualitative information on optically detectable, colloidally stable Ag-containing particles. Therefore, the absence of a plasmonic band cannot be used to exclude particulate release and should be interpreted together with total Ag release data and, where available, nanoparticle-specific methods such as spICP-MS. A sustained decline in wash-liquor Ag, alongside high on-fabric Ag retention, is consistent with strong anchoring typical of *in situ* synthesis.

To evaluate the possible release of Ag-containing species from the functionalized cotton during laundering, the washing water collected after 10 washing cycles was analysed using UV–vis spectroscopy, following previous reports in which LSPR monitoring was applied to AgNP-containing systems [64]. As shown in Fig. S2, the absorption band observed at ~250 nm is attributable to chitosan [40]. No distinct LSPR band near ~400 nm was detected; however, UV–vis is not a nanoparticle-specific release assay in complex wash liquors because detection requires sufficiently concentrated and colloidally stable AgNPs, whereas aggregation and matrix absorption/scattering can obscure an LSPR feature. In parallel, ICP-MS quantifies total Ag in the effluent after acidification/digestion and therefore does not distinguish dissolved Ag^+ from particulate Ag. Consequently, the UV–vis and ICP-MS results are not contradictory: the ICP-MS values demonstrate total silver wash-off, while the UV–vis data indicate that stable Ag-containing particulate species, if present, are below the UV–vis detection limit or not optically resolvable under the measurement conditions. Nanoparticle-specific release/speciation would require dedicated approaches such as spICP-MS or electron microscopy of extracted particulates [65,66]. These results suggest that, although loosely bound silver may be partially removed during washing, a substantial Ag-containing fraction remains associated with the substrate after multiple cycles.

3.5. Antibacterial efficacy

In light of the above considerations, the antibacterial activity of untreated and treated cotton fabrics was quantitatively evaluated against *S. aureus* and *E. coli* using the ASTM E2149-13a method, both before and after repeated laundering cycles (Fig. 6).

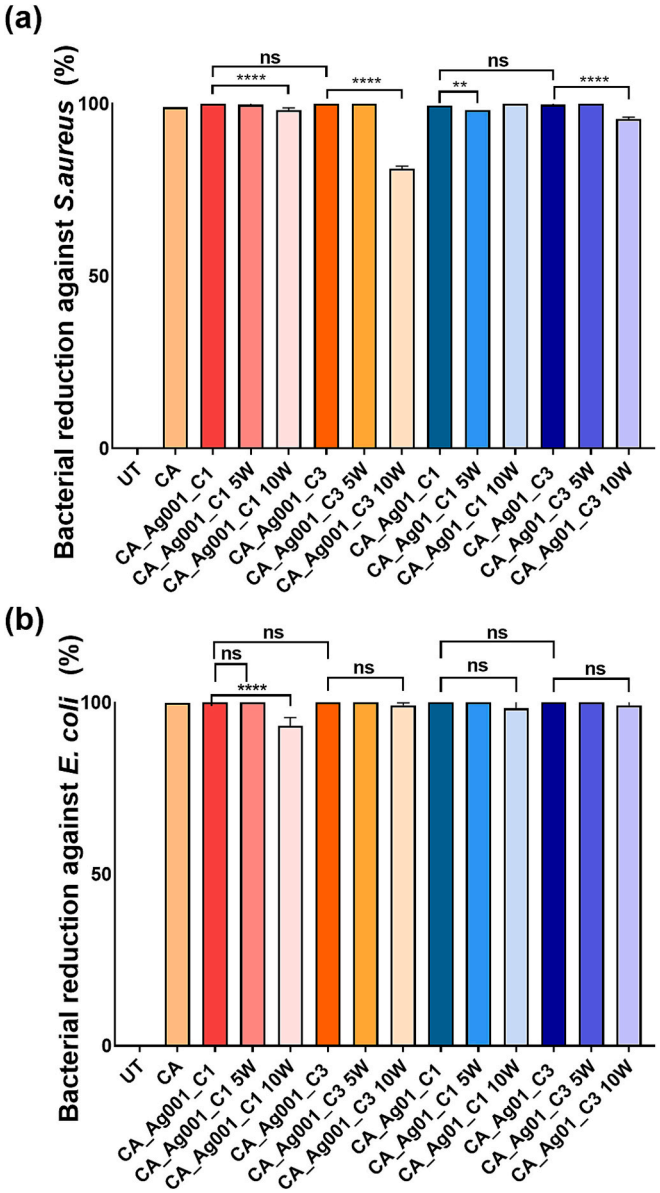

Fig. 6. Bacterial reduction (%) determined according to the ASTM E2149-13a standard against *S. aureus* (a) and *E. coli* (b) for untreated cotton (UT), citric-acid-treated cotton (CA), and Ag/chitosan-functionalized samples (CA_Ag001_C1, CA_Ag001_C3, CA_Ag01_C1, CA_Ag01_C3). UT and CA were evaluated in the unwashed state, whereas Ag/chitosan-functionalized samples were evaluated before washing and after 5 and 10 laundering cycles. Data are reported as mean ± SD. Statistical significance is indicated as ns (not significant), $p < 0.05$, $p < 0.01$, $p < 0.001$, $p < 0.0001$. The quantitative antibacterial reduction values supporting Fig. 6 are reported in **Table S1**, and representative agar plate images for selected *S. aureus* samples are provided in **Fig. S3**.

Untreated cotton (UT) showed no measurable reduction in bacterial count, confirming its lack of antimicrobial activity [67]. Citric-acid-treated cotton (CA), evaluated in the unwashed state, displayed high initial bacterial reduction (>99% for both strains), which is attributed here to a transient antibacterial effect associated with the acidic/chelating microenvironment generated by CA treatment rather than to a durable antimicrobial finish. Similar antimicrobial responses have been reported for CA/SHP-finished cotton under ISO 20743-type protocols, although they are strongly dependent on processing conditions, surface chemistry, and washing [68]. In the present work, the CA sample was not subjected to laundering because it represents the citric-acid-functionalized intermediate sample used for subsequent Ag loading and Ag/chitosan functionalization. Therefore, washing durability was assessed specifically for the Ag/chitosan-functionalized samples. The high antibacterial activity observed for the Ag/chitosan-functionalized samples reflects the formation of an effective Ag-based antimicrobial system stabilized within the chitosan matrix at the fibre surface [53,69]. After laundering, clear formulation-dependent differences emerged. The CA_Ag001_C1 sample retained high antibacterial efficacy after 10 washing cycles (98.1% against *S. aureus* and 93.2% against *E. coli*), indicating effective retention of the Ag-containing fraction on the cotton surface [70]. Increasing the chitosan concentration at the same Ag^+ level (CA_Ag001_C3) resulted in a more pronounced loss of activity against *S. aureus* after repeated washing, suggesting partial removal of loosely bound chitosan-silver domains [71]. Samples prepared with higher Ag^+ loading (CA_Ag01_C1 and CA_Ag01_C3) showed the most robust antibacterial durability, maintaining >95% bacterial reduction after 10 laundering cycles. This behaviour is consistent with a higher amount of Ag-containing domains and stronger association with the CA-functionalized cotton substrate [72,73]. Silver-release measurements during laundering further support this interpretation: higher initial silver release was observed for Ag-rich samples during early washes, followed by a marked decrease with increasing washing cycles, while low-Ag formulations exhibited consistently lower release values. Overall, the measured values fall within ranges previously reported for AgNPs-functionalized textiles and indicate predominant retention of Ag-containing species/domains within the cotton matrix [63]. More broadly, recent antibacterial cotton systems based on metal oxides, such as ZnO, have underscored the need for rigorous particle characterization and transparent microbiological validation when reporting high bacterial reductions [74]. Taken together, these results demonstrate that citric-acid-assisted Ag/chitosan functionalization yields cotton fabrics with high and durable antibacterial activity under standardized laundering conditions. While the present study focused on antibacterial efficacy and washing durability, cytocompatibility and long-term exposure aspects were beyond its scope and will be addressed in future work, in line with literature highlighting the dependence of silver-based textile safety on nanoparticle size, loading, and release behaviour [61,75–78].

Although the Ag^+ reduction step occurs at room temperature, the overall process includes a thermal curing stage (150 °C, 5 min) required for citric-acid grafting. This step represents the main energy input and is consistent with conventional pad-dry-cure textile finishing processes. Compared to alternative approaches, the proposed method avoids additional high-temperature or chemically intensive reduction steps, as AgNPs formation is achieved under ambient conditions using chitosan as a bio-based reducing and stabilizing agent. Therefore, the sustainability of the process should be interpreted in relative terms. A full life-cycle or energy-consumption assessment is beyond the scope of this work but will be considered in future studies.

From a process perspective, the proposed strategy is compatible with established textile finishing technologies. The citric-acid grafting step relies on a pad-dry-cure process, which is widely implemented at industrial scale and readily adaptable to continuous production lines. The subsequent Ag^+ uptake and chitosan treatment steps can be integrated using conventional aqueous processing routes, such as exhaustion or sequential padding with intermediate rinsing. Practical considerations include the need to control liquor ratios to ensure sufficient availability of Ag^+ during uptake, as well as managing chitosan solution properties, particularly viscosity and stability, to ensure uniform treatment. In addition, rinsing and wastewater handling represent relevant aspects for process scale-up. While these parameters were not systematically optimized in the present study, the overall workflow is inherently scalable and suitable for further development toward continuous or semi-continuous processing. In comparison with more advanced approaches, such as the microfluidic-assisted synthesis reported by Liu et al. [79], which enables the formation of smaller and highly uniform AgNPs (~13 nm) on alginate fibers with excellent long-term durability, the present method offers a simpler and more accessible alternative for cotton functionalization. Differences in substrate chemistry (carboxylated cotton *vs* alginate), reduction environment (chitosan-mediated room-temperature reduction *vs* UV/thermal-field-assisted synthesis), and particle size/distribution are expected to influence Ag release behaviour and antibacterial retention. In particular, smaller and more uniformly distributed AgNPs, as reported by Liu et al. [79], may provide more controlled release and enhanced durability, whereas the present cotton-based system, despite showing larger SEM-visible Ag-rich domains, achieves effective antibacterial performance and good washing resistance through *in situ* formation and strong anchoring within the functionalized cotton matrix. These considerations highlight the trade-off between precise nanoparticle control and process complexity, positioning the proposed approach as a practical route compatible with conventional textile finishing.

4. Conclusions

This study demonstrates the successful functionalization of cotton fabrics with Ag/chitosan-based antimicrobial domains *via* a chitosan-assisted *in situ* route, in which chitosan acts as a mild reducing and stabilizing agent according to literature-supported mechanisms. CIELAB colorimetric analysis revealed formulation-dependent variations in lightness, chromaticity, and K/S values, providing an initial optical indication of Ag-based surface functionalization, with higher silver loadings yielding darker and more intensely colored fabrics. SEM-EDX analyses confirmed the homogeneous distribution of predominantly spherical Ag-rich surface domains on the fibre surface, while FTIR and Raman spectroscopy demonstrated preservation of the main cellulose spectroscopic fingerprints, indicating that the fibre chemistry and morphology were largely retained at the probed scale. Mechanical testing further showed that the Ag/chitosan functionalization step did not induce significant additional changes in tensile strength or elongation beyond those associated with citric-acid grafting, supporting the surface-confined nature of the treatment. UV–vis analysis of wash liquors did not reveal a distinct LSPR signal attributable to stable Ag-containing species under the measurement conditions, while ICP-MS quantified total Ag release during laundering. Accordingly, the Ag/chitosan-functionalized fabrics exhibited durable antibacterial performance, with selected formulations maintaining >95% bacterial reduction against *Staphylococcus aureus* and *Escherichia coli* after 10 washing cycles. Overall, the synergistic combination of citric acid anchoring and chitosan-mediated Ag functionalization provides an effective strategy for producing laundering-resistant antibacterial cotton suitable for healthcare, hygiene, and protective textile applications. Future work will address cytocompatibility and complementary structural analyses to further support biomedical use.

CRediT authorship contribution statement

A. D'Agostino: Writing – original draft, Visualization, Validation, Methodology, Investigation, Formal analysis, Data curation, Conceptualization, Supervision, Writing – review & editing. **S. Facchiano:** Validation, Methodology, Formal analysis, Data curation. **C. Vineis:**

Visualization, Validation, Methodology. **M. Hadhri:** Validation, Methodology, Formal analysis. **R. Palucci Rosa:** Validation, Methodology, Formal analysis. **G. Rosace:** Visualization, Supervision, Conceptualization. **A. Safarshargh:** Validation, Methodology, Formal analysis. **V. Trovato:** Validation, Methodology, Formal analysis, Data curation.

Declaration of competing interest

The authors declare that they have no known competing financial interests or personal relationships that could have appeared to influence the work reported in this paper.

Acknowledgements

This work was funded by the National Plan for NRRP Complementary Investments (PNC, established with the decree-law 6 May 2021, n. 59, converted by law n. 101 of 2021) in the call for the funding of research initiatives for technologies and innovative trajectories in the health and care sectors (Directorial Decree n. 931 of 06-062022)- project n. PNC0000003- AdvaNced Technologies for Human-centrEd Medicine (project acronym: ANTHEM). This work reflects only the authors' views and opinions, neither the Ministry for University and Research nor the European Commission can be considered responsible for them.

Appendix A. Supplementary data

Supplementary data to this article can be found online at https://doi.org/10.1016/j.rechem.2026.103615.

Data availability

Data will be made available on request.

References

[1] T.M. Size, Share & Trends Analysis Report by Raw Material (Cotton, Wool, Silk, Chemical), by Product (Natural Fibers, Nylon), by Application (Technical, Fashion), by Region, and Segment Forecasts, 2022–2030, Gd. View Res. Доступу До Ресурсу Https//Www. Gd. Com/Industry-Analysis/Textile-Market, 2022.
[2] W. Liu, R. Zhang, G. Duan, L. Zhang, Y. Li, L. Yang, Bio-inspired and multifunctional polyphenol-coated textiles, Adv. Fiber Mater. 6 (2024) 952–977, https://doi.org/10.1007/s42765-024-00403-x.
[3] S. Babaeipour, P. Nousiainen, E. Kimiaei, J. Tienaho, N. Kohlhuber, R. Korpinen, K. Kaipanen, M. Österberg, Thin multifunctional coatings for textiles based on the layer-by-layer application of polyaromatic hybrid nanoparticles, Mater. Adv. 5 (2024) 6114–6131, https://doi.org/10.1039/D4MA00085D.
[4] A.P. Rananavare, R. Jain, J. Lee, Recent developments in superhydrophobic textiles: a status review, J. Coat. Technol. Res. 22 (2025) 549–580, https://doi.org/10.1007/s11998-024-01016-0.
[5] J. Ghosh, N.S. Rupanty, T. Noor, T.R. Asif, T. Islam, V. Reukov, Functional coatings for textiles: advancements in flame resistance, antimicrobial defense, and self-cleaning performance, RSC Adv. 15 (2025) 10984–11022, https://doi.org/10.1039/D5RA01429H.
[6] C. Colleoni, E. Guido, V. Migani, G. Rosace, Hydrophobic behaviour of non-fluorinated sol–gel based cotton and polyester fabric coatings, J. Ind. Text. 44 (2015) 815–834, https://doi.org/10.1177/1528083713516666.
[7] R. Dastjerdi, M. Montazer, A review on the application of inorganic nano-structured materials in the modification of textiles: focus on anti-microbial properties, Colloids Surf. B: Biointerfaces 79 (2010) 5–18, https://doi.org/10.1016/j.colsurfb.2010.03.029.
[8] S. Dixit, S. Varshney, D. Gupta, S. Sharma, Textiles as fomites in the healthcare system, Appl. Microbiol. Biotechnol. 107 (2023) 3887–3897, https://doi.org/10.1007/s00253-023-12569-2.
[9] J. Yao, S. Zheng, X. Wu, Y. Guo, Y. Li, Y. Mi, Z. Cao, Q. Cui, Durable antibacterial cotton fabrics based on synergy of bacterial repellence and bactericidal action, Colloids Surfaces A Physicochem. Eng. Asp. 677 (2023) 132408, https://doi.org/10.1016/j.colsurfa.2023.132408.
[10] L. Li, D. Zhou, J. Ye, K. Luan, Z. Zhang, L. Jing, T. Zhang, Long-lasting antibacterial cotton fabric treated with "one-bath" impregnation of N-halamine precursor, Chem. Eng. J. 512 (2025) 162290, https://doi.org/10.1016/j.cej.2025.162290.
[11] L.L. Ma, Y.Y. Wei, J. Li, Y.Y. Sun, S.R. Liu, K.M. Ma, P.-M. Leung, X.M. Tao, Clinical study of antibacterial medical textiles containing polyhydroxyalkanoate oligomers for reduction of hospital-acquired infections, J. Hosp. Infect. 149 (2024) 144–154, https://doi.org/10.1016/j.jhin.2024.04.009.
[12] N.E.-S. Ibrahim, Antimicrobial cotton fabrics, Nat. Rev. Bioeng. 1 (2023) 159, https://doi.org/10.1038/s44222-023-00048-2.
[13] O. Santoro, L. Izzo, Antimicrobial polymer surfaces containing quaternary ammonium centers (QACs): synthesis and mechanism of action, Int. J. Mol. Sci. 25 (2024) 7587, https://doi.org/10.3390/ijms25147587.
[14] A.R. Gomes, C.L. Varela, A.S. Pires, E.J. Tavares-da-Silva, F.M.F. Roleira, Synthetic and natural guanidine derivatives as antitumor and antimicrobial agents: A review, Bioorg. Chem. 138 (2023) 106600, https://doi.org/10.1016/j.bioorg.2023.106600.
[15] Z. Cui, Y. Wang, L. Zhang, H. Qi, Zwitterionic peptides: from mechanism, design strategies to applications, ACS Appl. Mater. Interfaces 16 (2024) 56497–56518, https://doi.org/10.1021/acsami.4c08891.
[16] S.R. Isbel, S.A. Patil, A. Bugarin, NHCs silver complexes as potential antimicrobial agents, Inorg. Chim. Acta 563 (2024) 121899, https://doi.org/10.1016/j.ica.2023.121899.
[17] B. Wang, G. Zhou, Q. Shi, W. Fan, X. Xie, Carbon dots as an emerging antibacterial agent: antibacterial mechanism and synthetic optimization, J. Environ. Chem. Eng. (2025) 118127, https://doi.org/10.1016/j.jece.2025.118127.
[18] S. Ali, A. Bahadur, A. Hassan, S. Ahmad, W. Shah, S. Iqbal, Optimized silver nanostructures for enhanced antibacterial potential: recent trends and challenges in the development of metallo-antimicrobials, Chem. Eng. J. 507 (2025) 160470, https://doi.org/10.1016/j.cej.2025.160470.
[19] E.L. Irede, R.F. Awoyemi, B. Owolabi, O.R. Aworinde, R.O. Kajola, A. Hazeez, A. A. Raji, L.O. Ganiyu, C.O. Onukwuli, A.P. Onivefu, Cutting-edge developments in zinc oxide nanoparticles: synthesis and applications for enhanced antimicrobial and UV protection in healthcare solutions, RSC Adv. 14 (2024) 20992–21034, https://doi.org/10.1039/D4RA02452D.
[20] P. She, S. Li, X. Li, H. Rao, X. Men, J. Qin, Photocatalytic antibacterial agents based on inorganic semiconductor nanomaterials: a review, Nanoscale 16 (2024) 4961–4973, https://doi.org/10.1039/D3NR06531F.
[21] A. Othman, A. Gowda, D. Andreescu, M.H. Hassan, S.V. Babu, J. Seo, S. Andreescu, Two decades of ceria nanoparticle research: structure, properties and emerging applications, Mater. Horiz. 11 (2024) 3213–3266, https://doi.org/10.1039/D4MH00055B.
[22] R. Abbas, J. Luo, X. Qi, A. Naz, I.A. Khan, H. Liu, S. Yu, J. Wei, Silver nanoparticles: synthesis, structure, properties and applications, Nanomaterials 14 (2024) 1425, https://doi.org/10.3390/nano14171425.
[23] A.S. Rodrigues, J.G.S. Batista, M.Á.V. Rodrigues, V.C. Thipe, L.A.R. Minarini, P. S. Lopes, A.B. Lugão, Advances in silver nanoparticles: a comprehensive review on their potential as antimicrobial agents and their mechanisms of action elucidated by proteomics, Front. Microbiol. 15 (2024) 1440065, https://doi.org/10.3389/fmicb.2024.1440065.
[24] V.S. Chandak, P.V. Nagime, Synthesis, characterization and applications of silver nanoparticles (Ag-NPs) in the field of electronics and optoelectronics device-a review, Hybrid Adv. (2025) 100389, https://doi.org/10.1016/j.hybadv.2025.100389.
[25] B. Sachdeva, K. Aggarwal, A. Singh, K. Kumari, R. Chandra, S. Singh, Advancements in silver-based nanocatalysts for organic transformations and other applications: a comprehensive review (2019–2024), RSC Adv. 15 (2025) 17591–17634, https://doi.org/10.1039/D5RA00336A.
[26] S.K. Mondal, S. Chakraborty, S. Manna, S.M. Mandal, Antimicrobial nanoparticles: current landscape and future challenges, RSC Pharm. 1 (2024) 388–402, https://doi.org/10.1039/D4PM00032C.
[27] G. Montes-Hernandez, M. Di Girolamo, G. Sarret, S. Bureau, A. Fernandez-Martinez, C. Lelong, E. Eymard Vernain, In situ formation of silver nanoparticles (Ag-NPs) onto textile fibers, ACS Omega 6 (2021) 1316–1327, https://doi.org/10.1021/acsomega.0c04814.
[28] M.E. El-Naggar, T.A. Khattab, M.S. Abdelrahman, A. Aldalbahi, M.R. Hatshan, Development of antimicrobial, UV blocked and photocatalytic self-cleanable cotton fibers decorated with silver nanoparticles using silver carbamate and plasma activation, Cellulose 28 (2021) 1105–1121, https://doi.org/10.1007/s10570-020-03537-4.
[29] M. Fahim, A. Shahzaib, N. Nishat, A. Jahan, T.A. Bhat, A. Inam, Green synthesis of silver nanoparticles: A comprehensive review of methods, influencing factors, and applications, JCIS Open 16 (2024) 100125, https://doi.org/10.1016/j.jciso.2024.100125.
[30] M.A. Dheyab, A.A.A. ziz, S.H. Nowfal, F.S. Braim, W. Abdullah, W.H. Kasasbeh, M. S. Jameel, S.T. Alanezi, M. Alrosan, N. Oladzadabbasabadi, Sustainable green synthesis of silver nanoparticles for safer biomedical application, J. Environ. Chem. Eng. (2025) 115998, https://doi.org/10.1016/j.jece.2025.115998.
[31] X. Gong, N.D. Jadhav, V.V. Lonikar, A.N. Kulkarni, H. Zhang, B.R. Sankapal, J. Ren, B. Bin Xu, H.M. Pathan, Y. Ma, An overview of green synthesized silver nanoparticles towards bioactive antibacterial, antimicrobial and antifungal applications, Adv. Colloid Interf. Sci. 323 (2024) 103053, https://doi.org/10.1016/j.cis.2023.103053.
[32] M. Hu, Q. Liu, D. Yang, Q. Wang, X. Chen, C. Chang, G. Zheng, Y. Meng, The factors influencing the synthesis of silver nanoparticles using natural polysaccharides, New J. Chem. 49 (2025) 10597–10607, https://doi.org/10.1039/D5NJ00430F.
[33] N. Pal, M. Agarwal, A. Ghosh, Green synthesis of silver nanoparticles using polysaccharide-based guar gum, Mater. Today Proc. 76 (2023) 212–218, https://doi.org/10.1016/j.matpr.2023.01.048.
[34] H.P. Syama, B.S. Unnikrishnan, J. Sreekutty, M.G. Archana, G.U. Preethi, P. L. Reshma, T.T. Sreelekha, Polysaccharide-capped silver nanoparticles impregnated cream for the efficient management of wound healing, RSC Pharm. 2 (2025) 570–580, https://doi.org/10.1039/D4PM00274A.

[35] L. Bonetti, A. Fiorati, A. D'Agostino, C.M. Pelacani, R. Chiesa, S. Farè, L. De Nardo, Smart methylcellulose hydrogels for pH-triggered delivery of silver nanoparticles, Gels 8 (2022) 298.

[36] P. Pallavicini, C.R. Arciola, F. Bertoglio, S. Curtosi, G. Dacarro, A. D'Agostino, F. Ferrari, D. Merli, C. Milanese, S. Rossi, Silver nanoparticles synthesized and coated with pectin: an ideal compromise for anti-bacterial and anti-biofilm action combined with wound-healing properties, J. Colloid Interface Sci. 498 (2017) 271–281, https://doi.org/10.1016/j.jcis.2017.03.062.

[37] P.K. Patel, R.V.S. Uppaluri, Chitosan and its functionalized derivatives for heavy metal ion elimination: A review of synthesis, mechanisms, and characterization studies, Adv. Colloid Interf. Sci. (2025) 103632, https://doi.org/10.1016/j.cis.2025.103632.

[38] K. Ahmad, Y. Zhang, P. Chen, X. Yang, H. Hou, Chitosan interaction with stomach mucin layer to enhances gastric retention and mucoadhesive properties, Carbohydr. Polym. 333 (2024) 121926, https://doi.org/10.1016/j.carbpol.2024.121926.

[39] H. Yadav, R. Malviya, N. Kaushik, Chitosan in biomedicine: A comprehensive review of recent developments, Carbohydr. Polym. Technol. Appl. 8 (2024) 100551, https://doi.org/10.1016/j.carpta.2024.100551.

[40] G.J.C. Canama, M.C.L. Delco, R.A. Talandron, N.P. Tan, Synthesis of chitosan-silver nanocomposite and its evaluation as an antibacterial coating for mobile phone glass protectors, ACS Omega 8 (2023) 17699–17711, https://doi.org/10.1021/acsomega.3c00191.

[41] N.P.U. Nguyen, N.T. Dang, L. Doan, T.T.H. Nguyen, Synthesis of silver nanoparticles: from conventional to 'modern'methods—a review, Processes 11 (2023) 2617, https://doi.org/10.3390/pr11092617.

[42] N.S. Mpofu, J.I. Mwasiagi, C.A. Mecha, E.O. Nganyi, Characterization and performance evaluation of cotton fabrics functionalized via in situ green synthesis of silver nanoparticles using *Solanum tuberosum* peel extract, Polymers (Basel) 17 (2025) 2598, https://doi.org/10.3390/polym17192598.

[43] A.P. Carapeto, A.M. Ferraria, A.M.B. do Rego, Unraveling the reaction mechanism of silver ions reduction by chitosan from so far neglected spectroscopic features, Carbohydr. Polym. 174 (2017) 601–609, https://doi.org/10.1016/j.carbpol.2017.06.100.

[44] A. Krkobabić, M. Radetić, H.-H. Tseng, T.S. Nunney, V. Tadić, T. Ilic-Tomic, D. Marković, Green in situ synthesis of ag-and cu-based nanoparticles on viscose fabric using a *Punica granatum* peel extract, Appl. Surf. Sci. 611 (2023) 155612, https://doi.org/10.1016/j.apsusc.2022.155612.

[45] International Organization for Standardization, IS/ISO 105-C10:2006; textiles-tests for colour fastness-part C10: colour fastness to washing with soap or soda and soda., 2006.

[46] T.S. Enstitüsü, Textiles-tensile properties of fabrics-part 1: determination of maximum force and elongation at maximum force using the strip method, Ankara, Türkiye 13934, 2013.

[47] Test Method for Determining the Antimicrobial Activity of Antimicrobial Agents Under Dynamic Contact Conditions, 2013, https://doi.org/10.1520/E2149-13A.

[48] P. Tang, B. Ji, G. Sun, Whiteness improvement of citric acid crosslinked cotton fabrics: H2O2 bleaching under alkaline condition, Carbohydr. Polym. 147 (2016) 139–145, https://doi.org/10.1016/j.carbpol.2016.04.007.

[49] Y. Yan, Y. Dong, L. Bian, Surface functionalization of cotton fabric with Ag3PO4 via citric acid modification using pad-dry-cure process for enhancing self-cleaning performance, Cellulose 29 (2022) 4203–4227, https://doi.org/10.1007/s10570-022-04507-8.

[50] C.Q. Yang, D. Chen, J. Guan, Q. He, Cross-linking cotton cellulose by the combination of maleic acid and sodium hypophosphite. 1. Fabric wrinkle resistance, Ind. Eng. Chem. Res. 49 (2010) 8325–8332, https://doi.org/10.1021/ie1007294.

[51] A. Abou-Okeil, Ag nanoparticles growing onto cotton fabric using chitosan as a template, J. Nat. Fibers 9 (2012) 61–72, https://doi.org/10.1080/15440478.2011.651841.

[52] C. Chung, M. Lee, E.K. Choe, Characterization of cotton fabric scouring by FT-IR ATR spectroscopy, Carbohydr. Polym. 58 (2004) 417–420, https://doi.org/10.1016/j.carbpol.2004.08.005.

[53] D. Wei, W. Sun, W. Qian, Y. Ye, X. Ma, The synthesis of chitosan-based silver nanoparticles and their antibacterial activity, Carbohydr. Res. 344 (2009) 2375–2382, https://doi.org/10.1016/j.carres.2009.09.001.

[54] Y.-K. Twu, Y.-W. Chen, C.-M. Shih, Preparation of silver nanoparticles using chitosan suspensions, Powder Technol. 185 (2008) 251–257, https://doi.org/10.1016/j.powtec.2007.10.025.

[55] B.S. Butola, A. Kumar, Green chemistry based in-situ synthesis of silver nanoparticles for multifunctional finishing of chitosan polysaccharide modified cellulosic textile substrate, Int. J. Biol. Macromol. 152 (2020) 1135–1145, https://doi.org/10.1016/j.ijbiomac.2019.10.202.

[56] D. Puchowicz, M. Cieslak, D. Puchowicz, M. Cieslak, Raman spectroscopy in the analysis of textile structures, Recent Dev. At. Force Microsc. Raman Spectrosc. Mater. Charact. (2022) 1–21.

[57] G. Dhiman, J.N. Chakraborty, Assessment of durable press performance of cotton finished with modified DMDHEU and citric acid, Fash. Text. 4 (2017) 18.

[58] P. Badanayak, J.V. Vastrad, S. Jose, Impact of polycarboxylic acid treatments on physico-mechanical properties of cotton fabric, Polym. Bull. 81 (2024) 12947–12965.

[59] A. Telli, M. Taş, In-situ functionalization of cotton fabrics with polydopamine and silver nanoparticles for multifunctional applications, Cellulose 32 (2025) 1377–1391.

[60] Q. Xu, E. Hu, H. Qiu, L. Liu, Q. Li, B. Lu, K. Yu, F. Lu, R. Xie, G. Lan, Catechol-chitosan/carboxymethylated cotton-based Janus hemostatic patch for rapid hemostasis in coagulopathy, Carbohydr. Polym. 315 (2023) 120967, https://doi.org/10.1016/j.carbpol.2023.120967.

[61] M. Rai, A. Yadav, A. Gade, Silver nanoparticles as a new generation of antimicrobials, Biotechnol. Adv. 27 (2009) 76–83, https://doi.org/10.1016/j.biotechadv.2008.09.002.

[62] Q. Xu, L. Xie, H. Diao, F. Li, Y. Zhang, F. Fu, X. Liu, Antibacterial cotton fabric with enhanced durability prepared using silver nanoparticles and carboxymethyl chitosan, Carbohydr. Polym. 177 (2017) 187–193, https://doi.org/10.1016/j.carbpol.2017.08.129.

[63] J. Hedberg, S. Skoglund, M.-E. Karlsson, S. Wold, I. Odnevall Wallinder, Y. Hedberg, Sequential studies of silver released from silver nanoparticles in aqueous media simulating sweat, laundry detergent solutions and surface water, Environ. Sci. Technol. 48 (2014) 7314–7322, https://doi.org/10.1021/es500234y.

[64] A. Taglietti, C.R. Arciola, A. D'Agostino, G. Dacarro, L. Montanaro, D. Campoccia, L. Cucca, M. Vercellino, A. Poggi, P. Pallavicini, Antibiofilm activity of a monolayer of silver nanoparticles anchored to an amino-silanized glass surface, Biomaterials 35 (2014) 1779–1788, https://doi.org/10.1016/j.biomaterials.2013.11.047.

[65] I. Rujido-Santos, M.E. del Castillo Busto, I. Abad-Alvaro, P. Herbello-Hermelo, P. Bermejo-Barrera, M.C. Barciela-Alonso, H. Goneaga-Infante, A. Moreda-Piñeiro, spICP-MS characterisation of released silver nanoparticles from (nano)textile products, Spectrochim. Acta Part B At. Spectrosc. 195 (2022) 106505, https://doi.org/10.1016/j.sab.2022.106505.

[66] I. Rujido-Santos, P. Herbello-Hermelo, M.C. Barciela-Alonso, P. Bermejo-Barrera, A. Moreda-Piñeiro, Metal content in textile and (nano)textile products, Int. J. Environ. Res. Public Health 19 (2022) 944, https://doi.org/10.3390/ijerph19020944.

[67] Y. Gao, R. Cranston, Recent advances in antimicrobial treatments of textiles, Text. Res. J. 78 (2008) 60–72, https://doi.org/10.1177/0040517507082332.

[68] S. Bischof Vukušić, S. Flinčec Grgac, A. Budimir, S. Kalenić, Cotton textiles modified with citric acid as efficient anti-bacterial agent for prevention of nosocomial infections, Croat. Med. J. 52 (2011) 68–75, https://doi.org/10.3325/cmj.2011.52.68.

[69] E. Susilowati, Maryani, Ashadi, Green synthesis of silver-chitosan nanocomposite and their application as antibacterial material, J. Phys. Conf. Ser. (2019) 12135, https://doi.org/10.1088/1742-6596/1153/1/012135. IOP Publishing.

[70] T. Jiang, L. Liu, J. Yao, In situ deposition of silver nanoparticles on the cotton fabrics, Fibers Polym. 12 (2011) 620–625, https://doi.org/10.1007/s12221-011-0620-4.

[71] H. Chen, G. Zhang, W. Zhang, W. Gao, Silver nanoparticles deposited on a cotton fabric surface via an in situ method using reactive hyperbranched polymers and their antibacterial properties, RSC Adv. 13 (2023) 11450–11456, https://doi.org/10.1039/D3RA00989K.

[72] J.R. Morones, J.L. Elechiguerra, A. Camacho, K. Holt, J.B. Kouri, J.T. Ramírez, M. J. Yacaman, The bactericidal effect of silver nanoparticles, Nanotechnology 16 (2005) 2346, https://doi.org/10.1088/0957-4484/16/10/059.

[73] Z. Zhang, L. Chen, J. Ji, Y. Huang, D. Chen, Antibacterial properties of cotton fabrics treated with chitosan, Text. Res. J. 73 (2003) 1103–1106, https://doi.org/10.1177/004051750307301213.

[74] S. Mahmoud, I. Alghoraibi, B. Younes, R. Zein, Development of antibacterial and hydrophobic cotton fabrics using zinc oxide and fluorocarbon nanocomposite, J. Text. Inst. 117 (2026) 585–596, https://doi.org/10.1080/00405000.2025.2515624.

[75] P.K. Dutta, S. Tripathi, G.K. Mehrotra, J. Dutta, Perspectives for chitosan based antimicrobial films in food applications, Food Chem. 114 (2009) 1173–1182, https://doi.org/10.1016/j.foodchem.2008.11.047.

[76] V.P. Veeraraghavan, N.D. Periadurai, T. Karunakaran, S. Hussain, K.M. Surapaneni, X. Jiao, Green synthesis of silver nanoparticles from aqueous extract of *Scutellaria barbata* and coating on the cotton fabric for antimicrobial applications and wound healing activity in fibroblast cells (L929), Saudi J. Biol. Sci. 28 (2021) 3633–3640, https://doi.org/10.1016/j.sjbs.2021.05.007.

[77] F. Paladini, C. Lanzillotti, A. Panico, M. Pollini, Biological evaluation of silver-treated silk fibroin scaffolds for application as antibacterial and regenerative wound dressings, Nanomaterials 15 (2025) 919, https://doi.org/10.3390/nano15120919.

[78] M. Akter, M.T. Sikder, M.M. Rahman, A.K.M.A. Ullah, K.F.B. Hossain, S. Banik, T. Hosokawa, T. Saito, M. Kurasaki, A systematic review on silver nanoparticles-induced cytotoxicity: physicochemical properties and perspectives, J. Adv. Res. 9 (2018) 1–16, https://doi.org/10.1016/j.jare.2017.10.008.

[79] H. Liu, X. Lan, Y. Yin, X. Wang, X. Chen, J. Zhou, K. Chen, X. Zhang, Green synthesis and durable antibacterial AgNP-loaded alginate fibers enabled by microfluidic technology coupled with ultraviolet/thermal fields, ACS Appl. Polym. Mater. 7 (2025) 5259–5270, https://doi.org/10.1021/acsapm.5c00655.